AFRL-RD-PS-TP-
2009-1006

Photon Noise in Digital Holographic Detection

Joseph C. Marron

Lockheed Martin Coherent Technologies
135 S. Taylor Ave.
Louisville, CO 80027

01 September 2008

Technical Paper

APPROVED FOR PUBLIC RELEASE; DISTRIBUTION IS UNLIMITED.

AIR FORCE RESEARCH LABORATORY
Directed Energy Directorate
3550 Aberdeen Ave SE
AIR FORCE MATERIEL COMMAND
KIRTLAND AIR FORCE BASE, NM 87117-5776

THIS PAGE INTENTIALLY LEFT BLANK

REPORT DOCUMENTATION PAGE

Form Approved
OMB No. 0704-0188

Public reporting burden for this collection of information is estimated to average 1 hour per response, including the time for reviewing instructions, searching existing data sources, gathering and maintaining the data needed, and completing and reviewing this collection of information. Send comments regarding this burden estimate or any other aspect of this collection of information, including suggestions for reducing this burden to Department of Defense, Washington Headquarters Services, Directorate for Information Operations and Reports (0704-0188), 1215 Jefferson Davis Highway, Suite 1204, Arlington, VA 22202-4302. Respondents should be aware that notwithstanding any other provision of law, no person shall be subject to any penalty for failing to comply with a collection of information if it does not display a currently valid OMB control number. **PLEASE DO NOT RETURN YOUR FORM TO THE ABOVE ADDRESS.**

1. REPORT DATE *(DD-MM-YYYY)*	2. REPORT TYPE	3. DATES COVERED *(From - To)*
01-09-2008	Technical Paper	Sept 2006- Sept 2008

4. TITLE AND SUBTITLE
Photon Noise in Digital Holographic Detection

5a. CONTRACT NUMBER
FA9451-06-C-0376 DF297714

5b. GRANT NUMBER

5c. PROGRAM ELEMENT NUMBER
6TRDSE

6. AUTHOR(S)
Joseph C. Maroon

5d. PROJECT NUMBER
6255

5e. TASK NUMBER
SU

5f. WORK UNIT NUMBER
AB

7. PERFORMING ORGANIZATION NAME(S) AND ADDRESS(ES)
Lockheed Martin Coherent Technologies
135 S. Taylor Ave
Louisville, CO 80027

8. PERFORMING ORGANIZATION REPORT NUMBER

9. SPONSORING / MONITORING AGENCY NAME(S) AND ADDRESS(ES)
Air Force Research Laboratory
3550 Aberdeen Ave SE
Kirtland AFB NM 87117-5776

10. SPONSOR/MONITOR'S ACRONYM(S)
AFRL/RDSEA

11. SPONSOR/MONITOR'S REPORT NUMBER(S)
AFRL-RD-PS-TP-2009-1006

12. DISTRIBUTION / AVAILABILITY STATEMENT
Approved for Public Release

13. SUPPLEMENTARY NOTES
Submitted for publication in Optics Express; June 2009; Washington, DC.
"GOVERNMENT PURPOSE RIGHTS"

14. ABSTRACT
Digital holographic detection is used to measure coherent, complex-valued image or pupil-plane data. With the complex-valued data, one has access to digital representation of the optical field and therefore can perform advanced functions such as three-dimensional imaging and correction of phase errors imparted by instrumentation or atmospheric turbulence. This paper contains a derivation of the signal to noise ratio specifically for digital holographic detection in the presence of photon noise and shows that quantum-limited detection and stellar speckle interferometry. An example signal-to-noise calculation is included with a discussion of quadrature detection.

15. SUBJECT TERMS

16. SECURITY CLASSIFICATION OF:			17. LIMITATION OF ABSTRACT	18. NUMBER OF PAGES	19a. NAME OF RESPONSIBLE PERSON
a. REPORT	b. ABSTRACT	c. THIS PAGE			Dan Marker
Unclassified	Unclassified	Unclassified	SAR	16	19b. TELEPHONE NUMBER *(include area code)* 505-846-2871

Photon Noise in Digital Holographic Detection

Joseph C. Marron
Lockheed Martin Coherent Technologies
135 S. Taylor Ave.
Louisville, CO 80027

Abstract

Digital holographic detection is used to measure coherent, complex-valued image or pupil-plane data. With the complex-valued data, one has access to a digital representation of the optical field and therefore can perform advanced functions such as three-dimensional imaging and correction of phase errors imparted by instrumentation or atmospheric turbulence. This paper contains a derivation of the signal to noise ratio specifically for digital holographic detection in the presence of photon noise and shows that quantum-limited detection is achieved as expected from similar analysis for temporal heterodyne detection and stellar speckle interferometry. An example signal-to-noise calculation is included with a discussion of quadrature detection.

1.0 Introduction

Shortly after the invention of lasers and optically recorded holography, researchers demonstrated the ability to record holographic interference patterns on a 2D detector array and recover images by digital Fourier transformation [1]. Improvements in laser power and coherence, detector arrays, and computer processing have led to the application of digital holography to numerous fields. Applications of digital holographic detection to distant objects was also conducted several years ago [2], but again, advancements in laser and detector technologies have enabled additional capabilities including obtaining three-dimensional imaging by recording a series of digital holograms at different wavelengths [3, 4] and correction of phase errors imparted by optical instrumentation and atmospheric turbulence [5, 6, 7]. In applying digital holographic detection to imaging of distant objects one is often limited by the return light level. In this paper we concentrate on the application of digital holography to the recovery complex-valued image data and present a derivation of the signal-to noise- ratio.

Another method often used to determine coherent or complex-valued information from distant objects is temporal heterodyne detection [8] which has been applied extensively to the measurement of wind velocity [9]. Temporal heterodyne detection is the temporal analogue to digital holographic detection and sometimes digital holographic detection is called spatial heterodyne detection. The remarkable property of temporal heterodyne detection is that it allows one to perform photon-limited detection of signals that are dominated by detector or background noise. This is accomplished by having a strong local oscillator. As shown herein, this property also applies to digital holography where instead of boosting the strength of the local oscillator, one analogously boosts the strength of the reference beam.

While the SNR calculation for digital holography is analogous to heterodyne detection, it is more complicated because of the 2D nature of the signals. For calculation of the SNR for digital holography researchers often refer to a related calculations for speckle interferometry summarized in Ref. [10]. This paper contains thorough calculation of the SNR specifically for digital holography and demonstrates that under low light conditions, the unwanted autocorrelation term is negligible which has significant impact on detector sampling requirements. We also discuss the implications of quadrature detection. A sample SNR calculation for imaging distant objects is included.

2.0 Digital Holography

An example digital holographic detection system for imaging distant objects is shown in Fig. 1. Here the object is flood illuminated with coherent light from a laser source. The return light propagates to the detector array. A beamsplitter is used to insert light from a point source; this point source serves as the reference point source for holographic recording. These two coherent beam components, object and reference, then interfere at the detector and the intensity of the interference pattern is recorded by the detector array.

Visual inspection of the recorded intensity pattern reveals that for a deterministic point object that is located at the same conjugate distance as the reference point, one sees a distinct sinusoid corresponding to the interference of the point object with the reference point. The spatial frequency of this sinusoid can be analyzed using conventional Fourier optics treatments of two-beam interference. It follows that close separations of the object and local oscillator points produce fringes with low spatial-frequencies and conversely, large separations produce high spatial-frequencies. An example of the sinusoidal intensity pattern that results from a point object interfering with the local oscillator is shown in Fig. 3.

The recorded intensity for a diffuse object is a random pattern that is often called a speckle pattern because of its random, granular appearance. For this case the object field consists of a collection of points with deterministic locations and random amplitudes and phases. When the random object field components are mixed with a reference point having a sufficient spatial offset, the resulting intensity pattern has a speckled appearance with a modulation, or carrier frequency, evident within each speckle. An example speckle pattern from a 2D, circular disk object is shown in Fig. 3.

Following intensity detection, the next step in the detection process is to compute the digital Fourier transform. The Fourier transform of the speckle intensity above is shown in Fig. 4.

Notice that there are 3 image terms evident in Fig. 4; two twin disk images with a larger disk in the center. Additionally there is a bright point in the center, but this has been digitally zeroed in Fig. 4 so that the other image terms are visible. To understand these image terms let us denote the disk object as f and the reference point as g with their corresponding Fourier transforms given by F and G respectively. The intensity recorded by the detector array can be written as

$$I = |(F+G)|^2$$
$$= |F|^2 + |G|^2 + FG^* + F^*G. \quad (1)$$

It follows that the Fourier transform of this intensity is given by

$$FT(I) = f \otimes f^* + g \otimes g^* + f \otimes g^* + f^* \otimes g, \quad (2)$$

where $\otimes$ denotes the convolution operation. If the reference point is a delta function centered at $x=b$, it follows that the Fourier transform of the intensity pattern is given by

$$FT(I) = f \otimes f^* + \delta(x) + f(x-b) + f^*(x+b). \quad (4)$$

Note the correspondence between the terms of Eq. (4) and Fig. 4. The first term in Eq. (4) is the autocorrelation of the object; for the disk object this corresponds to the central tapered disk in Fig. 4. The second term is a delta function at the origin that is zeroed as discussed above. The final two terms are a set of twin images spatially offset from the center by $\pm b$. These images are complex-valued and by extracting one of them, for example the boxed region in Fig. 4, the complex-valued representation of the object field is obtained.

In order to extract the complex valued image term, the angular offset of the reference beam should be large enough so that the image terms do not overlap with the autocorrelation term. However, in the case of a weak object return and strong local oscillator, the autocorrelation term can be negligible when compared to the strength of the image term and thus overlap can be tolerated. This consideration has important implications for hardware design and will be discussed further below in the context of low object returns.

In summary, the basic digital holographic detection process is composed of the following steps:

1) Light from an object is interfered with light from a coherent, spatially-offset reference beam and the intensity is recorded.
2) The Fourier transform of the recorded intensity pattern is computed.
3) The complex-valued object field is obtained by extracting a subsection of the Fourier transform. The location of the subsection is determined by the angular separation of the object and reference beam components.

As stated above, the information contained in the complex valued image enables subsequent processing steps such as image refocusing, turbulence correction or 3D imaging.

3.0 Signal-to-Noise Ratio

A feature of digital holographic detection is that the image terms in Eq. (2) are proportional to the strength of the reference component multiplied by the strength of the object component. Thus, even if the object return is weak it can be boosted by using a strong reference beam. In the analysis below we will derive expressions for the SNR and concentrate on the weak object field case. To simplify notation below we abbreviate local

oscillator as LO and since the local oscillator is analogous to the reference beam we use LO to refer to the reference beam in digital holographic detection.

As we begin this analysis, consider an example case that includes the effects of photon noise. A convenient quantity for characterizing the object return strength is the number of photons per detector pixel in an array detector shown for example in Fig. 1. The size of the detector pixel is ideally matched to the Nyquist frequency limit which depends on the object size and spatial carrier frequency or LO angular offset. These sampling considerations will be discussed below in Section 4. Consider a disk object for which the return level is 100 photons per pixel. Also consider an LO level of 10^5 photons per pixel. Note that the selection of LO level is typically chosen relative to the electron well capacity of the detector pixel; exceeding the well capacity results in detector saturation.

An example of the recorded intensity pattern for the low-return case described above is shown in Fig. 5 below. Note the reduced contrast and granular appearance of the pattern relative to the high-return case shown in Fig. 3. While this data seems noisy, the corresponding Fourier transform, shown in Fig. 6, reveals a quality image.

An important feature of the image shown in Fig. 6 is that the central term corresponding to the object's autocorrelation is not visible. This is because the image terms are amplified by the LO signal level, as mentioned above, whereas the autocorrelation term is not. The absence of the autocorrelation is especially serendipitous because one can employ lower spatial carrier frequencies while still achieving separation of the image terms appearing in the autocorrelation. This feature is discussed further in Section 4 below.

Another visible feature is that Fig. 6 appears to have a higher noise bias than Fig. 4. This noise bias is caused by the photon noise (shot noise) in the LO. In fact the SNR for digital holography is a quantification of the image strength relative to this photon noise bias.

To compute the SNR consider the case of a deterministic point object. We can write the optical field in the object plane as two delta functions, one from the object at lateral location a and one from the reference beam at lateral location b. The strengths of the delta function fields are the square roots of their intensities given by I_S and I_{LO} for the object and local oscillator respectively. Let us also include a relative phase, ϕ, on the object. We can then write the optical field in the object plane as

$$U(x) = \sqrt{I_S}\exp(i\phi)\delta(x-a) + \sqrt{I_{LO}}\delta(x-b). \tag{5}$$

Propagation of the optical field to the detector plane in the far field corresponds to a Fourier transform in the arrangement shown in Fig. 1. The field at the detector is then

$$U(\xi) = \kappa\left(\sqrt{I_S}\exp(i(\phi - \frac{2\pi}{\lambda R}\xi a)) + \sqrt{I_{LO}}\exp(-i\frac{2\pi}{\lambda R}\xi b)\right), \tag{6}$$

where κ is an inessential constant that we can ignore at this point. We can now write the intensity signal recorded by the detector array as

$$d(\xi) = \frac{\eta\tau}{h\nu}(P_S + P_{LO} + P_B) + \tag{7}$$
$$+ \frac{\eta\tau}{h\nu}\sqrt{P_{LO}}\sqrt{P_S}\left(\exp\left[i(\phi - \frac{2\pi}{\lambda R}\xi(a-b))\right] + \exp\left[-i(\phi - \frac{2\pi}{\lambda R}\xi(a-b))\right]\right),$$

where P_S and P_{LO} are the powers per detector pixel with an additional bias term, P_B, added to represent the uniform background contribution from dark current to each pixel. The factor $\eta\tau/h\nu$ converts from incident power to output signal in units of photoelectrons where η is the detector quantum efficiency, τ is the integration time and $h\nu$ is the photon energy.

With detector output, we can now move to step 2 of the digital holography process and compute the inverse Fourier transform of the recorded intensity. This gives

$$D(s) = \frac{\eta\tau}{h\nu}(P_S + P_{LO} + P_B)\delta(s) + \tag{8}$$
$$+ \frac{\eta\tau}{\mathrm{hv}}\sqrt{P_{LO}}\sqrt{P_S}\left(\exp(i\phi)\delta\left[s - \frac{2\pi}{\lambda R}(a-b)\right] + \exp(-i\phi)\delta\left[s + \frac{2\pi}{\lambda R}(a-b)\right]\right).$$

If we evaluate this expression at $s = \frac{2\pi}{\lambda R}(a-b)$ we find

$$D\left(\frac{2\pi}{\lambda R}(a-b)\right) = \frac{\eta\tau}{h\nu}\sqrt{P_{LO}}\sqrt{P_S}\exp(i\phi). \tag{9}$$

The presence of the phase and amplitude shows that the complex-valued signal can indeed be determined by evaluating the Fourier transform of the detected intensity pattern at the corresponding location and that the signal strength is boosted by the local oscillator strength.

To evaluate the noise level, consider the constant terms in Eq. (7). It follows that the dominant noise source is the photon noise that originates from these constants; this gives rise to the noise 'floor' that is visible in Fig. 6. To determine the magnitude of this noise, let us also regard the signal as being composed of a series of photoevents that occur at discrete locations in the detection plane. For simplicity let us combine the bias terms into a single quantity $P = P_{LO} + P_s + P_B$. Following Ref. 10 we write the contribution from this term as a summation of K photoevents occurring at locations ξ_n or

$$d(\xi) = \sum_{n=1}^{K}\delta(\xi - \xi_n). \tag{10}$$

K is related to P by

$$K = \frac{NP\eta\tau}{h\nu}, \tag{11}$$

where N is the total number of detectors.

Now consider the Fourier transform of d which is the second step in the digital holographic detection process. We have

$$D(s) = \frac{1}{\sqrt{N}} \int \sum_{n=1}^{K} \delta(\xi - \xi_n) \exp(-i2\pi\xi s) d\xi$$
$$= \frac{1}{\sqrt{N}} \sum_{n=1}^{K} \exp(-i2\pi\xi_n s) \tag{12}$$

which shows that $D(s)$ is a sum of a series of random phasors indicating that the noise is zero-mean Gaussian in nature. The $\sqrt{N}$ normalizing constant follows from Parseval's theorem. To evaluate the noise level in the transform, we take the expected value of $|D|^2$ or

$$\langle |D(s)|^2 \rangle = \frac{1}{N} \langle \sum_{m=1}^{K} \sum_{n=1}^{K} \exp(-i2\pi s(\xi_n - \xi_m)) \rangle . \tag{13}$$

Note that there are two types of terms in Eq. (13); K diagonal terms for which $n=m$ and the phasor reduces to unity. And there are the remaining K^2-K non-diagonal terms for which we need to compute the expected value of the phase term in Equation (13). Using the probability density function of the spatial distribution of the photoevents, $p(\xi_m, \xi_n)$ we have

$$\langle \exp(-i2\pi s(\xi_m - \xi_n)) \rangle = \int \int p(\xi_m, \xi_n) \exp(-i2\pi s(\xi_m - \xi_n)) d\xi_m d\xi_n . \tag{14}$$

For the non-diagonal case of $n \neq m$, $p(\xi_m, \xi_n) = p(\xi_m) p(\xi_n)$ giving

$$\langle \exp(-i2\pi s(\xi_m - \xi_n)) \rangle = \int p(\xi_m) \exp(-i2\pi s(\xi_m) d\xi_m \int p(\xi_n) \exp(i2\pi s(\xi_n)) d\xi_n . \tag{15}$$

Inspection of the right hand side of Eq. (15) reveals that it is equivalent to the squared magnitude of the characteristic function [1] where the characteristic function is defined to be the Fourier transform of the probability density function. Also, because the spatial distribution of the photoevents is typically uniform over the detector array, the characteristic function reduces to a delta function at $s=0$. This gives

$$\langle |D(s)|^2 \rangle = \frac{1}{N} \left(K + (K^2 - K) \delta(s) \right). \tag{16}$$

For this analysis we can ignore the location $s=0$ because measurements at this location are not useful. It then follows that the noise background is given by

$$\langle |D(s \neq 0)|^2 \rangle = K/N , \tag{17}$$

which indicates that this background noise intensity is uniform over the image (as observed in Fig. 5) and is proportional to the total number of photons received divided by the number of detectors.

This SNR for measurement of the intensity of a point using digital holographic detection is the ratio of the signal given by the squared magnitude of Eq. (9) and the noise given by Eq. (17) which yields

$$SNR = \frac{\eta P_{LO} P_s \tau}{h\nu (P_{LO} + P_S + P_B)} , \tag{18}$$

For the case of the background and signal being dominated by the local oscillator, Eq. (18) becomes

$$SNR = \eta P_s \tau / h\nu, \tag{19}$$

which corresponds to quantum-limited detection and agrees with results for conventional heterodyne detection [2]. Note here that P_s is the power per detector pixel, and thus the SNR is given by the number of photons per detector pixel.

4.0 Sampling Considerations

Fielded systems are typically designed so that the detector array pixels sample the received light at the Nyquist sampling limit. If we assume that the pixel size is equal to the pixel separation, it follows that sampling finer that the Nyquist frequency results in an unnecessary reduction in SNR and sampling more coarsely than the Nyquist frequency results in image aliasing.

To achieve Nyquist sampling in the detection system shown in Fig. 1, one would match the detector pixel size to the maximum spatial frequency incident on the detector array which depends on the maximum apparent angular offset between the signal and local oscillator beams. For the case of high object-return level, an object of width W would be separated from the local oscillator by a lateral distance equal to W so that the object and autocorrelation terms do not overlap. This separation is sometimes called the holography condition. In this case the detector spacing, or size, is given by

$$S_{HOLOGRAPHY} = \lambda R / 4W, \tag{20}$$

where λ is the source wavelength, R is the range to the object and W is the object width. Equation 20 corresponds to one-fourth of the average speckle width or speckle size [11].

As demonstrated in Fig. 6, for the low-signal case one can reduce the angular offset so that the local oscillator is at the edge of the object boundary. In this case the apparent maximum angular separation of the object and local oscillator is reduced and thus the Nyquist sample spacing is increased so that the detector pixel size for the low-light level case is given by

$$S_{LOW-LIGHT} = \lambda R / 2W, \tag{21}$$

which corresponds to one half of the speckle size.

A further increase in the detector pixel size can realized if quadrature detection is employed. Quadrature detection involves recording a series of digital holograms with the phase of the local oscillator shifted [3] and then the digital holograms are algebraically combined to isolate a single, complex-valued image term. This same principal is used in phase shifting interferometry and it is common to use 4 values for the local oscillator phase: 0, $\pi/2$, π and $3\pi/2$ however other versions involving fewer or more phase values have been developed [12]. With quadrature detection the detector pixel size becomes

$$S_{QUADRATURE} = \lambda R / W, \tag{22}$$

which is equal to the speckle size.

Equations (20-22) indicate that quadrature detection can provide the best SNR because the detector pixels are the largest and thus the number of photons per detector pixel is largest. This advantage, however, comes at the cost of the increased instrumentation complexity required for phase shifting. Also, if the quadrature frames are collected as a temporal sequence the data can experience temporal decorrelation under dynamic situations. One other point is that the algebraic combination of the frames used in quadrature detection does improve the SNR via averaging; however, this same advantage applies to non-quadrature detection if multiple realizations of photon noise are used.

5.0 SNR Example

Consider the case of imaging an object of width W that is located at a distance of R. Let us represent the object reflectivity as ρ and assume that the object reflects diffusely with Lambertian weighting and that the system is near monostatic. Also, consider the low-light case with the detector size given by Eq. (21). For a laser illumination power P, it follows that the signal level P_S is given by

$$P_S = \frac{P\lambda^2\rho}{4\pi W^2}. \tag{23}$$

Substitution of Eq. (23) into Eq. (19) gives

$$SNR = \frac{\eta\tau P\lambda^3\rho}{4hc\pi W^2}. \tag{24}$$

For a specific case, let us consider illumination of a distant object with a 10 mJ laser pulse; thus τP = 10 mJ. Other parameters are: η = 0.8, λ = 1.0 μm, and ρ = 0.1. Also let us take the object size to be W=5 m and the distance R=1 km. From Eq. (21) we find that the detector size is 100 μm and from Eq. (23) it follows that for this scenario SNR = 12.8.

Note that in practice the detector pixels size required for Nyquist sampling can be larger (or smaller) than the detector pixel size for commercially available detectors. In this case a simple relay optical system is used to re-image pupil-plane speckle data onto the detector array with the appropriate magnification.

Also note that anamorphic optics or asymmetric detector pixels can be used with holographic and low-light detection systems to better match the detector sizes to the intensity pattern and thereby improve the SNR. Such improvements are not considered in this analysis.

6.0 Conclusion

This paper contains a derivation of the SNR for digital holographic detection. It is shown that the method is capable of quantum limited detection when the intensity of the

reference point dominates the background intensity level. This conclusion corresponds to the analogous result obtained for temporal heterodyne detection.

Acknowledgement

This paper was prepared with partial support from Lockheed Martin Internal Research and Development funding and funding from the Air Force Research Laboratory under contract FA9451-06-C-0376.

References

1. J. W. Goodman and R. W. Lawrence, "Digital Image Formation from Electronically Detected Holograms," Applied Physics Letters, 11, 77-79, 1967.
2. J. W. Goodman, D. W. Jackson, M. Lehmann, J. Knotts, 'Experiments in Long-Distance Holographic Imagery', Appl. Opt., 8, 1581-1586, 1969.
3. J. C. Marron and K. S. Schroeder, "Three-Dimensional Lensless Imaging Using Laser Frequency Diversity," Applied Optics, 31, 255-262, 1992.
4. J. C. Marron and K. S. Schroeder, "Holographic Laser Radar," Optics Letters, 18, 385-387, 1993.
5. R. G. Paxman and J. C. Marron, "Aberration Correction of Speckled Imagery With an Image Sharpness Criterion," In Proceedings of the SPIE Conference on Statistical Optics, 976, San Diego, CA, August 1988.
6. J. R. Fienup and J. J. Miller, "Aberration Correction by Maximizing Generalized Image Sharpness Metrics," J. Opt. Soc. Am, A, 20,609-620, 2003.
7. J. C. Marron, R. L. Kendrick "Distributed Aperture Active Imaging,", In Proc. SPIE, Conference on Laser Radar, 6550, Orlando, FL, April 2007.
8. A. Yariv, *Introduction to Optical Electronics*, (Holt, Rhinehart and Winston, New York, 1977, Section 11.4).
9. S. Henderson, P. Gatt, D. Rees, and R. M. Huffaker, "Wind Lidar", in Laser Remote Sensing, Takashii Fujii and Tetsuo Fukuchi, ed., (CRC Press, Boca Raton, Florida, 2005).
10. J. W. Goodman, *Statistical Optics*, (John Wiley and Sons, New York, 1984, Section 9.6).
11. J. W. Goodman, "Statistical Properties of Laser Speckle Patterns," in Laser Speckle and Related Phenomenon, J.C. Dainty, ed., (Springer-Verlag, Berlin, 1984).
12. J. E. Greivenkamp and J. H. Bruning, "Phase shifting interferometers," in Optical Shop Testing, D. Malacara, ed. (Wiley, New York, 1991), Chap. 14, pp. 501–598.

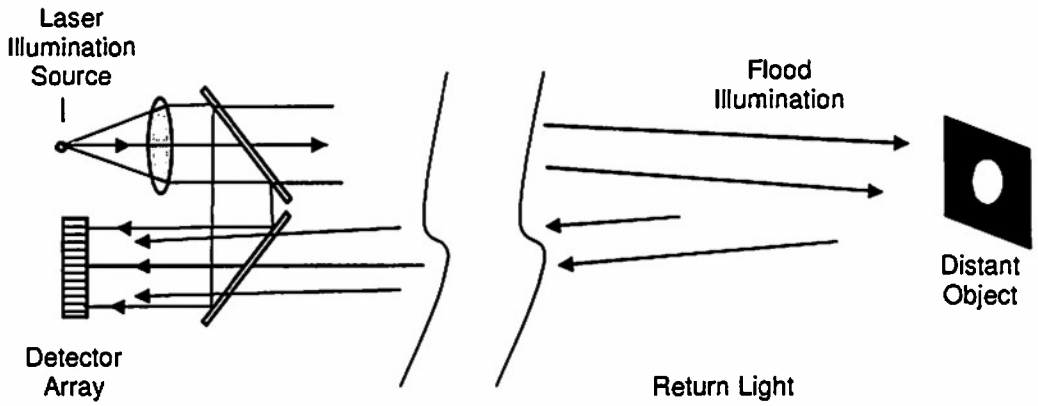

Figure 1. Example measurement configuration for digital holographic detection of distant objects.

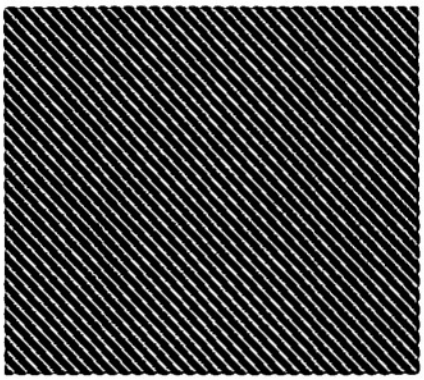

Figure 2. Example sinusoidal intensity pattern that results from interference of point object with point local oscillator.

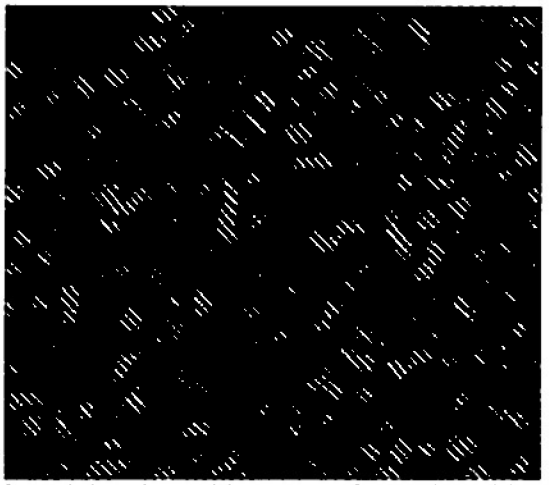

Figure 3. Example of modulated speckle pattern from disk object with spatially offset local oscillator.

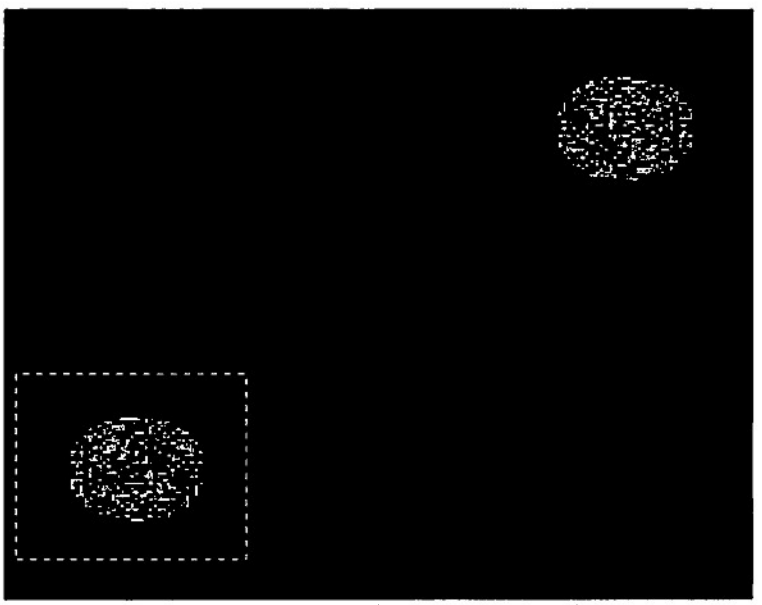

Figure 4. Fourier transform of speckle intensity from disk object and local oscillator.

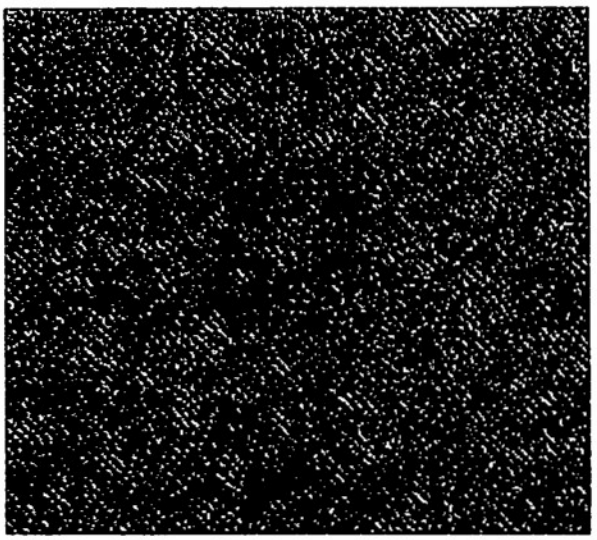

Figure 5. Speckle pattern corresponding to low object signal level (100 photons per detector pixel) and high LO level (10^5 photons per detector pixel).

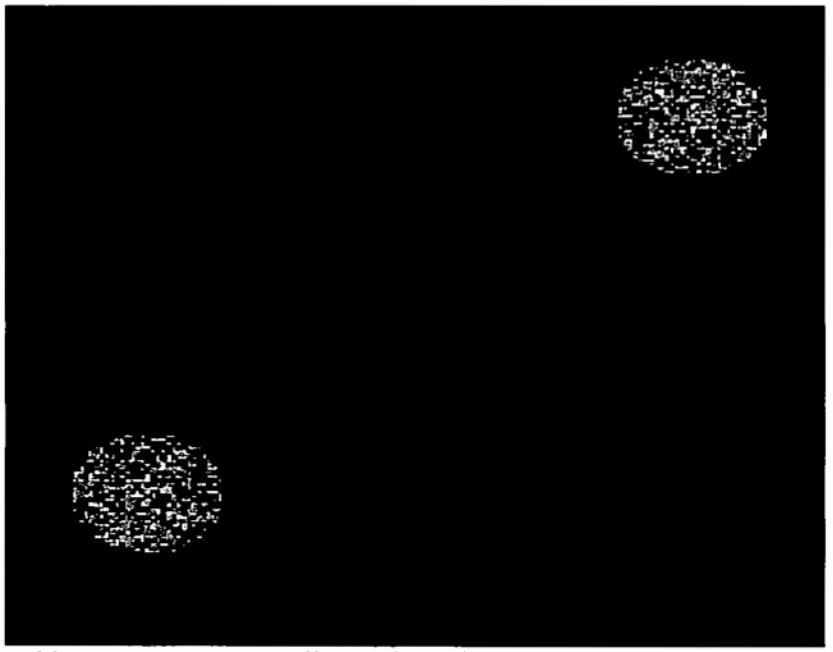

Figure 6. Speckle pattern corresponding to low object signal level (100 photons per detector pixel) and high LO level (10^5 photons per detector pixel).